Bioresource Technology 289 (2019) 121664

Contents lists available at ScienceDirect

Bioresource Technology

journal homepage: www.elsevier.com/locate/biortech

Characteristics of the extracellular polymeric substance composition in an up-flow biological aerated filter reactor: The impacts of different aeration rates and filter medium heights

Jiehui Ren, Wen Cheng*, Tian Wan, Min Wang, Ting Meng, Taotao Lv

State Key Laboratory of Eco-hydraulics in Northwest Arid Region of China, Xi'an University of Technology, NO. 5, South Jinhua Road, Xi'an, Shaanxi 710048, PR China

GRAPHICAL ABSTRACT

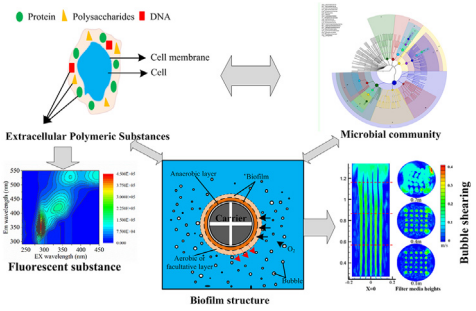

ARTICLE INFO

Keywords:
Aeration rates
Filter medium
Microbial community
Fluorescent substance
UBAF

ABSTRACT

In this study, the compositional characteristics of extracellular polymeric substances (EPS) were systematically explored to reveal their relationship with microbial community under different conditions in an up-flow biological aerated filter reactor. The aeration rates had a significant positive correlation ($0.898 \leq R \leq 0.979$) with the tightly bound (TB)-EPS contents, but basically showed an opposite trend ($R < -0.631$) with the loosely bound (LB)-EPS. Moreover, the filter medium heights also affected EPS distribution. The microbial biofilm produced more LB-EPS and TB-EPS to withdraw from the extreme environment. Five fluorescent substances were identified in the EPS by EEM-PARAFAC modeling; namely, two protein-like components (protein-like C1 and tryptophan-like C2) and three humic-like components (UVA marine humic-like C3, hydrophobic humic acid-like C4, and humic acid-like C5). Under different conditions, the relative abundance of *Proteobacteria* and *Nitrospirae* had a significant positive correlation with C5 and C4, respectively. These results demonstrated that microbial community distribution could affect EPS composition.

1. Introduction

The up-flow biological aerated filter (UBAF) reactor has good application prospects in municipal wastewater treatment as a fixed-film process, owing to its compact structure, ease of operation, low sludge production, high environmental shock resistance, and efficiency in the removal of carbon and ammonia (Tao et al., 2016). Previous researchers have studied the pollutant removal efficiency of UBAFs, optimization of the reactor structure, and the distribution of microbial community (Abu Hasan et al., 2013; He et al., 2018; Tao et al., 2016; Yang et al., 2016). The microbial biofilm plays an important role in the pollutant removal and reactor operation. However, research on the

* Correspondent author.
E-mail address: wencheng@xaut.edu.cn (W. Cheng).

https://doi.org/10.1016/j.biortech.2019.121664
Received 4 May 2019; Received in revised form 13 June 2019; Accepted 15 June 2019
Available online 18 June 2019
0960-8524/

characteristics of biofilms in UBAFs is not sufficiently comprehensive, and in-depth and comprehensive research on biofilm properties are therefore required.

The major components of biofilm are the microorganisms and the extracellular polymeric substances (EPS) (Miao et al., 2018), that they excrete as products of various cellular processes (e.g., metabolism, biomass growth, and decay) (Maqbool et al., 2016). These EPS play essential roles in the mechanical stability, surface adhesion, and formation of the biofilms itself (Flemming et al., 2016; Flemming and Wingender, 2010; Sheng et al., 2010; Shi et al., 2017). Several studies have demonstrated that EPS can affect the performance of wastewater treatment by changing biofilm characteristics (Sheng et al., 2010; Shi et al., 2017; Wang et al., 2018). Characterizing the compositions and variations of the EPS can thus help understanding the mechanism of pollutant removal and explain the potential drivers behind biofilm functions (Miao et al., 2018). However, there are no known research that have explored the compositions and contents of EPS in the UBAF reactor.

Previous studies of EPS have focused mostly on their compositions (Sheng and Yu, 2006; Yang and Li, 2009; Wang et al., 2018; Yu et al., 2009; Zhu et al., 2013), fluorescence characteristics (Baghoth et al., 2011; Maqbool et al., 2016; Sheng and Yu, 2006; Xu et al., 2013; Yu et al., 2015;), extraction method (Keithley and Kirisits, 2018), dewatering performance (Cao et al., 2018; Shao et al., 2009; Zhang et al., 2015), and membrane pollution control (Nagaraj et al., 2018; Shi et al., 2017). Miao et al. (2018) found that changes in the anammox bacteria were basically consistent with the variation in EPS composition. Moreover, they indicated that the microbial community could change the composition and concentration of EPS. However, few studies have explored the relationship between the EPS composition and microbial community structure, despite that in-depth research of the relationship could help understanding the mechanism of pollutant treatment and to optimize the stable operation of UBAF reactors.

The amounts and compositions of EPS were found to be affected by various operational parameters of the biofilms process (Shammi et al., 2017). In the UBAF reactor system, aeration is an important operational parameter, playing roles in the supply of dissolved oxygen and the growth of the biofilm. In addition, a suitable aeration rate could increase the removal efficiency of pollutants and reduce the energy consumption of the system (Rezakazemi et al., 2011). Previous studies found that a high aeration rate could increase the shearing force of the ceramsite surface and the velocity of the liquid phase (Ren et al., 2018a). Abu Bakar et al. (2018) indicated that a high-water velocity will increase the shearing of the biofilm surface and the production of EPS. Furthermore, an increase in the EPS contents could stabilize the biofilm structure and allow it to withstand the shear force. Therefore, the compositions and contents of EPS under different aeration rates should be deeply analyzed for a better understanding of the relationship between biofilm functions and the microbial community structure.

In this study, the compositions and contents of EPS in a UBAF reactor were analyzed to determine the effects of different aeration rates and filter medium heights on the biofilm properties. Three-dimensional excitation–emission matrix (EEM) fluorescence spectroscopy and EEM-PARAFAC modeling were used to explore the fluorescence properties of each EPS fraction. The microbial community structures under the different reactor conditions were also investigated. Redundancy analysis (RDA) was applied to analyze the relationship between the EPS compositions and microbial community structure. Such compositional characterization of the EPS and microbial communities could help understanding the functions of the biofilm in the UBAF reactor.

2. Materials and methods

2.1. Laboratory-scale UBAF reactor and operation

The experiment was carried out in a laboratory-scale UBAF reactor with a filter medium layer of 0.85 m in height and 0.35 m in diameter, and a working volume of 0.06 m^3 (see Supplementary data). The details of the device have been described in a previous paper (Ren et al., 2018b). The UBAF reactor was fed synthetic wastewater, which was prepared from tap water enriched with $C_6H_{12}O_6$ as a carbon source, NH_4Cl and KNO_3 as nitrogen sources, $K_3PO_4{\cdot}3H_2O$ as a phosphorus source, and $CaCl_2$, $MgSO_4{\cdot}5H_2O$, $NaHCO_3$, and $FeCl_3$ as trace element sources. Inoculated sludge was collected from a secondary sedimentation tank (Xi'an Third Wastewater Plant, Xi'an, China). The activated sludge was cultivated for one week before inoculation, and the nutrient medium was replaced every day. The synthetic wastewater was based on the contamination levels in domestic wastewater, and its characteristics are listed in Supplementary data.

2.2. EPS extraction method

The EPS matrix can be divided into three parts, namely, the soluble EPS (SL-EPS), loosely bound EPS (LB-EPS), and tightly bound EPS (TB-EPS) (Xu et al., 2013). Heat extraction and centrifugation were used for the extraction of the three parts. The extraction method used had been proven to be able to obtain the EPS with relatively high efficiency and low cell lysis (Baghoth et al, 2011; Xu et al., 2013). In this study, the biofilm samples were first centrifuged at 4000 r/min for 5 min, whereupon the supernatant was filtered and collected as the SL-EPS fraction. Next, the filtered biofilm samples were suspended in a 0.05% NaCl solution (50 °C) and centrifuged at 10,000 r/min for 15 min. The supernatant was filtered and collected as the LB-EPS fraction. Finally, the remaining biofilm samples were suspended in a 0.50% NaCl solution and then heated at 70 °C for 40 min. The samples were centrifuged at 10000r/min for 15 min, and the supernatant that was subsequently filtered was considered the TB-EPS fraction. All the supernatant samples were filtered using 0.45 μm Nylon66 membrane filters (Jinlong, Keyilong Experimental Equipment Co., Ltd., Tianjin, China), with the filtered solutions analyzed for EPS concentrations and fluorescence.

2.3. EPS analysis method

The protein (PN), polysaccharide (PS), and nucleic acid (DNA) contents were used to represent the extraction efficiency of each EPS fraction. The EPS level was analyzed according to the method described by Yu et al. (2009). The PN content was determined by the modified Lowry method, using bovine serum albumin (A116563-5g, Aladdin, Shanghai Jingchun Biochemical Technology Co., Ltd., Shanghai, China) as the standard substance. The PS content was measured by the anthrone method, using glucose as the standard substance. The DNA content was determined by the diphenylamine colorimetric method, with calf thymus DNA (C119712, Aladdin, Shanghai Jingchun Biochemical Technology Co., Ltd., Shanghai, China) as the standard substance. The total suspended solids and volatile suspended solids (VSS) were measured according to previously described standard methods (Yu et al., 2009). The EPS concentration is expressed in the amount of substance per gram of organic matter, and the unit is mg/g VSS.

2.4. Excitation-emission matrix analysis

The FluoroMax-4 spectrofluorometer was applied for detecting the fluorescent substances in the EPS samples. The fluorescent substances mainly included protein-like components, tryptophan, humic acid, and fulvic acid (Sheng et al., 2013). EEM spectra were gathered in the scanning emission (Em) range of 290–550 nm at 2-nm increments by varying the excitation (Ex) wavelength from 240 to 450 nm at 2-nm increments. The slit width was 3 nm for all samples.

2.5. EEM-PARAFAC modeling

PARAFAC modeling was carried out by analyzing the EEM

fluorescence data with the DOMFluor/PARAFAC toolbox in Matlab R2014a (Mathworks, Natick, MA, USA) (Stedmon and Bro, 2008). As suggested by Stedmon and Bro (2008), parameters with non-negative constraints were applied to allow only chemically relevant results. The pretreatment process was used to minimize the scattering effect and other properties of the EEM. The EEM result for Milli-Q water was treated as the background value and subtracted from all the EPS samples. Other Rayleigh and Raman scattering effects were also deducted. The treatments described above reduced the influence of the EPS concentrations on the component matrix. The EEM data were calculated using the 2–7 components of the PARAFAC model. The correct number of components was mainly determined by residual analysis and visual inspection (Liu et al., 2017).

2.6. Microbial community analysis

The biofilm of the filter medium was detached from its surface in the UBAF reactor. Biofilms of filter medium at different aeration rates (1.11×10^{-5} m^3/s, 1.81×10^{-5} m^3/s, and 2.50×10^{-5} m^3/s) and layer heights (0.1 m, 0.4 m, and 0.7 m) were also collected. The samples from different aeration rates (1.11×10^{-5} m^3/s, 1.81×10^{-5} m^3/s, and 2.50×10^{-5} m^3/s) were taken from reactor operated with a filter medium height of 0.85 m, and those from different filter medium heights (0.1 m, 0.4 m, and 0.7 m) were taken from reactor operated with an aeration rate of 2.50×10^{-5} m^3/s. DNA was extracted using a PowerBiofilm™ DNA Isolation kit for biofilm (Mo Bio, Carlsbad, CA, USA) and stored at − 20 °C. In addition, the microbial community structure was further analyzed with high-throughput sequencing technology, using Illumina Hiseq 2000 from the Shanghai Personal Biotechnology Co., Ltd. (Shanghai, China).

2.7. Statistical analysis

SPSS 22.0 for Windows (SPSS Inc., Chicago, IL, USA) was used for all statistical analyses. Pearson's correlation analysis was performed to determine the relationships between the aeration rates and EPS contents, with significance levels set at $p < 0.05$ (*) and $p < 0.01$ (**). The correlation coefficient R was also determined.

CANOCO 4.5 software was applied to analyze the relationships among the aeration rates, filter medium heights, EPS contents, and microbial community structure. First, the longest gradient of the detrended correspondence analysis was < 3.0 (Zhang et al., 2018). The result indicated that the linear model was more suitable for the aeration rates, filter medium heights, EPS contents, and microbial community. Hence, RDA was conducted to link the changes of the microbial community with the environmental variables and EPS contents.

3. Results and discussion

3.1. Effects of aeration rates on the contents and compositions of EPS

Fig. 1 shows the variations of EPS contents at different aeration rates in the UBAF reactor, where T-EPS represents the total content of each fraction and equaled the sum of the SL-EPS, LB-EPS, and TB-EPS at the same aeration rate. As shown in Fig. 1, the contents of PN in the EPS matrix were higher than those of PS and DNA. The concentrations of PN, PS, and DNA were 141.33–178.64 mg/g VSS, 52.4–89.36 mg/g VSS, and 6.09–9.62 mg/g VSS, respectively, and were consistent with results from previous studies (Shao et al., 2009; Wang et al., 2018). He et al. (2018) reported that the higher production of PN over PS might contribute to maintenance of the structure and stability of the EPS matrix. In addition, the contents of the EPS showed an increasing trend from SL-EPS to TB-EPS. The distribution was related to the EPS structure.

The aeration rates significantly affected the contents of each fraction in the EPS matrix. The concentration of TB-EPS had a significant positive correlation ($R \geq 0.898$, $p \leq 0.001$) with the aeration rates. When the aeration rate was 2.50×10^{-5} m^3/s, the PN, PS, and DNA concentrations were 141.80 ± 0.50 mg/g VSS, 71.98 ± 2.71 mg/g VSS, and 6.57 ± 0.23 mg/g VSS, respectively. The main reason for this is because a high aeration rate induces the biofilm to produce more EPS, which could stabilize the biofilm structure and allow it to withstand the shearing force (Abu Bakar et al., 2018). The PN and PS concentrations of the SL-EPS and LB-EPS had a negative correlation ($-0.976 \leq R \leq -0.744$, $0.0001 \leq p \leq 0.022$) with the aeration rates. The EPS distribution was mainly related to the shearing effect of aeration. A previous report had indicated that a higher aeration rate formed higher shearing in the filter medium surface of the UBAF reactor (Ren et al., 2018a). The higher shearing force would lead to the outer layer of EPS being stripped from the microbial cell surface. The DNA concentration at the aeration rate of 1.81×10^{-5} m^3/s was 9.62 ± 0.35 mg/g VSS, being significantly higher than that at the other conditions. Previous research found that the UBAF reactor achieved higher pollutant removal at the aeration rate of 1.81×10^{-5} m^3/s (Ren et al., 2018b). In addition, this condition increased the diversity of the microbial community. These results showed that the aeration rate of 1.81×10^{-5} m^3/s might promote the metabolic activity of the microbes.

3.2. Effects of filter medium height on the contents and compositions of EPS

The distribution of the EPS concentrations at different filter medium heights is shown in Fig. 2. The concentrations of PN at the different filter medium heights were significantly higher those of PS and DNA. In addition, the concentrations of PN and DNA had a negative correlation ($-0.999 \leq R \leq -0.250$, $1.1 \times 10–6 \leq p \leq 0.516$) with the filter medium heights. The total concentrations of PN and DNA at the filter medium height of 0.10 m reached to 141.71 ± 0.52 mg/g VSS and 9.92 ± 0.26 mg/g VSS, respectively. The results might be related to the abundance and diversity of the microbes, which previous research had found to be significantly higher at the bottom of the filter medium layer than at the other layers (Ren et al., 2018b). However, PS had a positive correlation ($-0.237 \leq R \leq 0.785$, $0.012 \leq p \leq 0.677$) with the filter medium heights, where its concentration (35.11 ± 5.09 mg/g VSS) at the height of 0.70 m was significantly higher than that at the other heights. He et al. (2017) indicated that EPS could serve as a carbon source for biological processes under extreme conditions. At the bottom of the filter medium layer, the higher abundance and diversity of the microbial community would mean a greater requirement of carbon sources for growth and metabolism. Because part of the PS might be treated as a carbon source by microbes, the PS concentration was reduced at this layer.

The concentrations of PN, PS, and DNA in the LB-EPS were basically similar to those in the LB-EPS at the different filter medium heights. However, the contents of TB-EPS were significantly higher those of SL-EPS and LB-EPS. These results might be related to the microbial community and ambient conditions. Compared with the EPS contents at the different aeration rates, those at the different filter medium heights showed a significant difference. The LB-EPS, TB-EPS, and T-EPS contents at the different filter medium heights were higher than those at the different aeration rates, whereas the SL-EPS contents presented the opposite trend. This might be related to differences in the metabolic activity of the microbes. The biofilm samples from reactors at different aeration rates were taken from the filter medium height of 0.85 m. The dissolved oxygen content (8.56–8.99 mg/L) at this position was significantly higher than that under the other filter medium heights (0.90–1.71 mg/L) (Ren et al., 2018a), indicating that the microbial community structure might have changed. On the other hand, previous studies found that the shearing force of the ceramsite surface increased at the filter medium height of 0.85 m (Ren et al., 2018a). The high shearing force could reduce the concentration of SL-EPS and increase the production of LB-EPS and TB-EPS. These results indicated that the

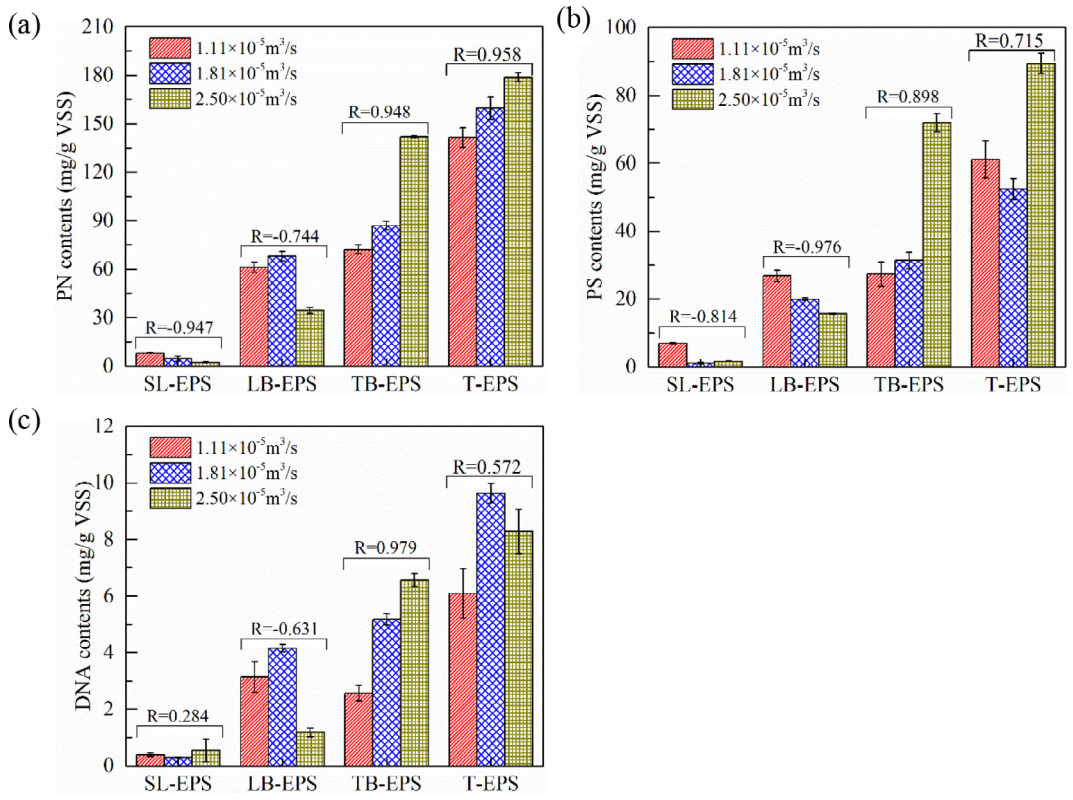

Fig. 1. Variations of protein (PN), polysaccharide (PS), and DNA in the EPS matrix under different aeration rates: (a) Distribution of PN; (b) Distribution of PS; (c) Distribution of DNA.

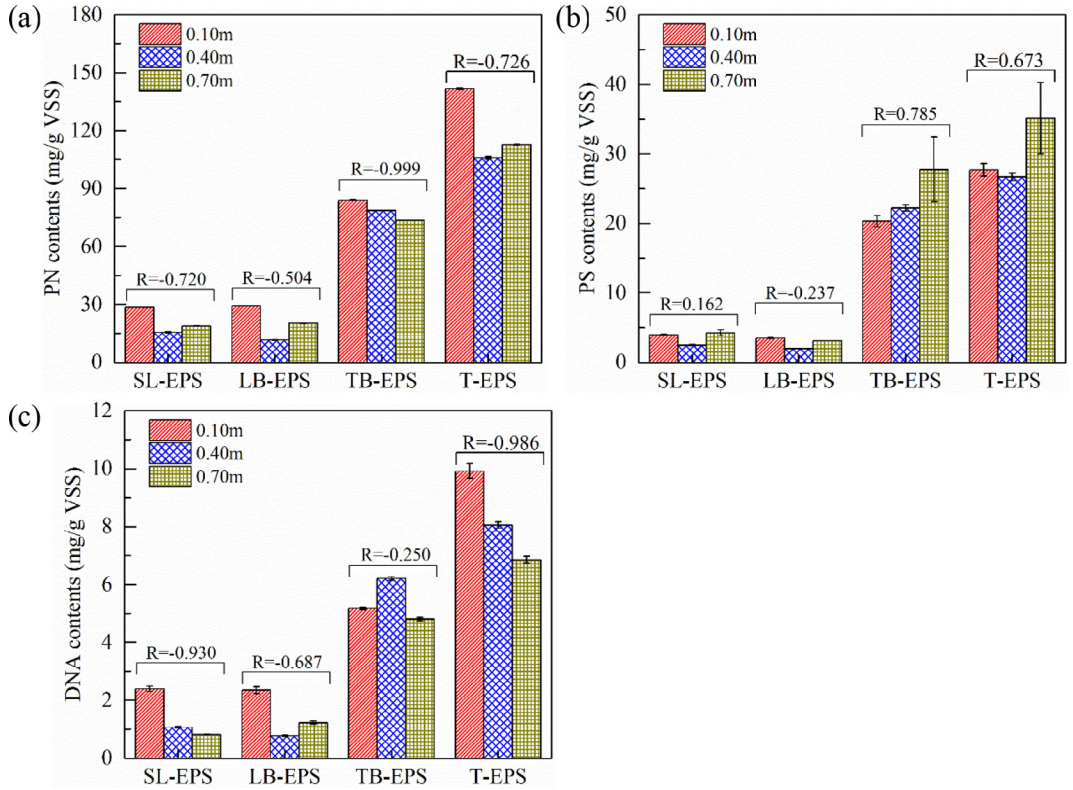

Fig. 2. Variations of protein (PN), polysaccharide (PS), and DNA in the EPS matrix under different filter medium heights: (a) Distribution of PN; (b) Distribution of PS; (c) Distribution of DNA.

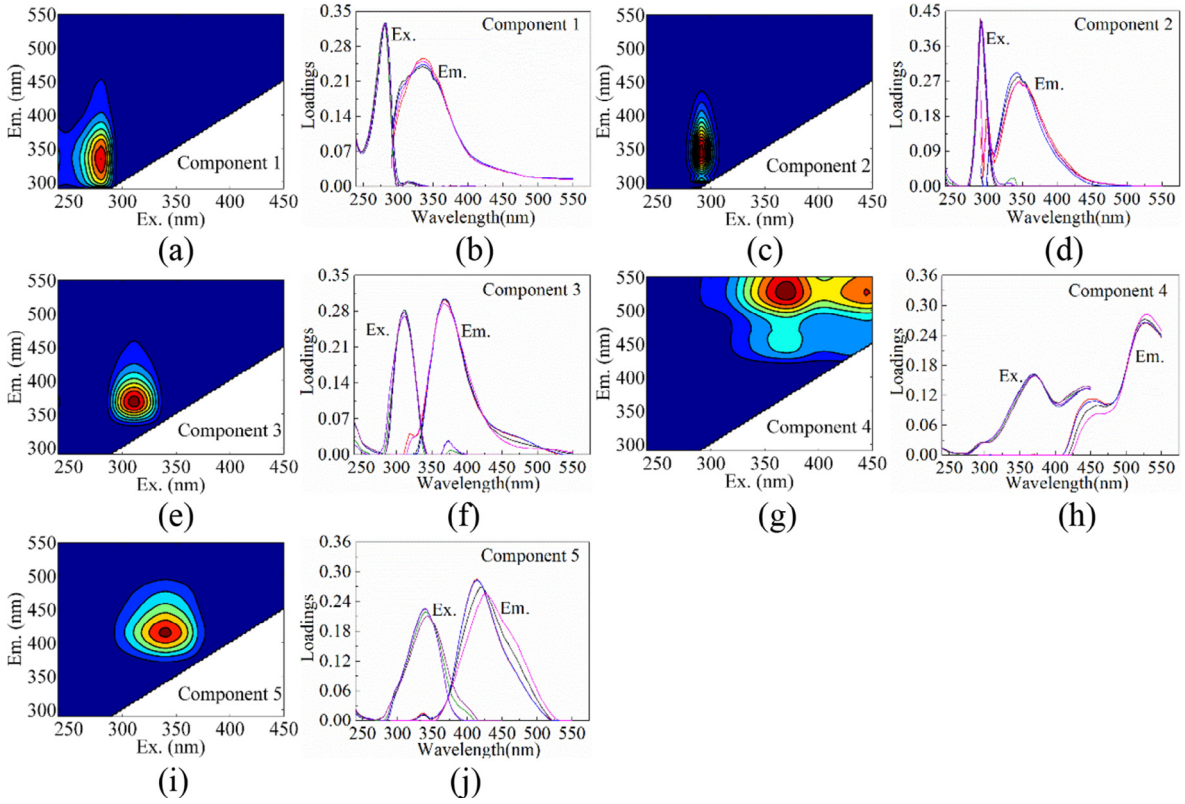

Fig. 3. EEM-PARAFAC results for Component 1 (C1), Component 2 (C2), Component 3 (C3), Component 4 (C4), and Component 5 (C5) and the split-half validation: The contour plots (Fig. 3(a), (c), (e), (g), and (i)) represent the spectral shapes of excitation (Ex) and emission (Em) of soluble (SL)-EPS, loosely bound (LB)-EPS, and tightly bound (TB)-EPS. The line plots (Fig. 3(b), (d), (f), (h), and (j)) represent the split-half validation results.

high production of LB-EPS and TB-EPS could help the biofilm to withdraw from the effects of the external environment.

3.3. Three-dimensional EEM contour of each EPS fraction

A total of 18 fluorescence EEM contours for the EPS samples under the different aeration rates and filter medium heights are depicted in Supplementary data. The EEM contours of TB-EPS showed four fluorescence peaks under the different conditions. However, SL-EPS and LB-EPS showed different fluorescence peaks (four peaks, two peaks, or one peaks) under the different conditions, indicating that these two fractions might be significantly affected by the external environment. EEM-PARAFAC modeling was applied to distinguish the fluorescent components. The results of CompareSpecSSE indicated that the 5-component model was more suitable for the analysis of EPS fluorescent substances in biofilms (see Supplementary data). In addition, the results of split-half validation (see Supplementary data) further verified the suitability of the model.

Fig. 3 presents the results of the fluorescent components and split-half validation of samples extracted under different aeration rates and filter medium heights. Previous studies (Table 1) showed the presence of five components, consisting of two protein-like substances and three humic-like substances. C1, with its Ex/Em peak at 280/334 nm, was identified as a protein-like substance (Cao et al., 2018; Yu et al., 2015). C2, which exhibited a single Ex/Em peak at 290/344 nm, was assigned to a tryptophan-like substance (Murphy et al., 2011). It was notable that C1 and C2 were classified as protein-like components that were related to biological production and microbial community activity (Lu et al., 2009; Xu et al., 2013). C3 was located at the Ex/Em peak of 312/368 nm. Fluorescence in this region is attributed to UVA marine humic-like substances, which are mainly derived from anthropogenic wastewater (Coble, 2007; Stedmon et al., 2011). C4 (Ex/Em = 374(442)/532 nm) and C5 (Ex/Em = 350/440 nm) were identified as hydrophobic humic acid-like and humic acid-like substances, respectively,

Table 1
Spectral characteristics of the five components identified by PARAFAC analysis in this study and in previous studies.

This study		Previous studies		
Components	Ex/Em	Ex/Em	Description	References
C1	280/334	280/330–340	Protein-like substance	Seredyńska-Sobecka et al. (2011); Yu et al. (2015)
		280/335	Protein	Cao et al. (2018)
C2	290/344	290/352	Tryptophan-like	Murphy et al. (2011)
		280–285/340–350	Protein	Sheng and Yu (2006)
C3	312/368	290–310/370–410	UVA marine humic-like	Coble (2007)
		315/384	Marine humic-like	Stedmon et al. (2011)
C4	374(4 4 2)/532	240–275(339–420)/434–520	Hydrophobic Humic acid-like	Ishii and Boyer (2012)
C5	350/440	(230–260, 320–350)/420–450	Humic substances	Cao et al. (2018); Qu et al. (2012)
		350/443.5–445	Humic acid-like substances	Wei et al. (2017)

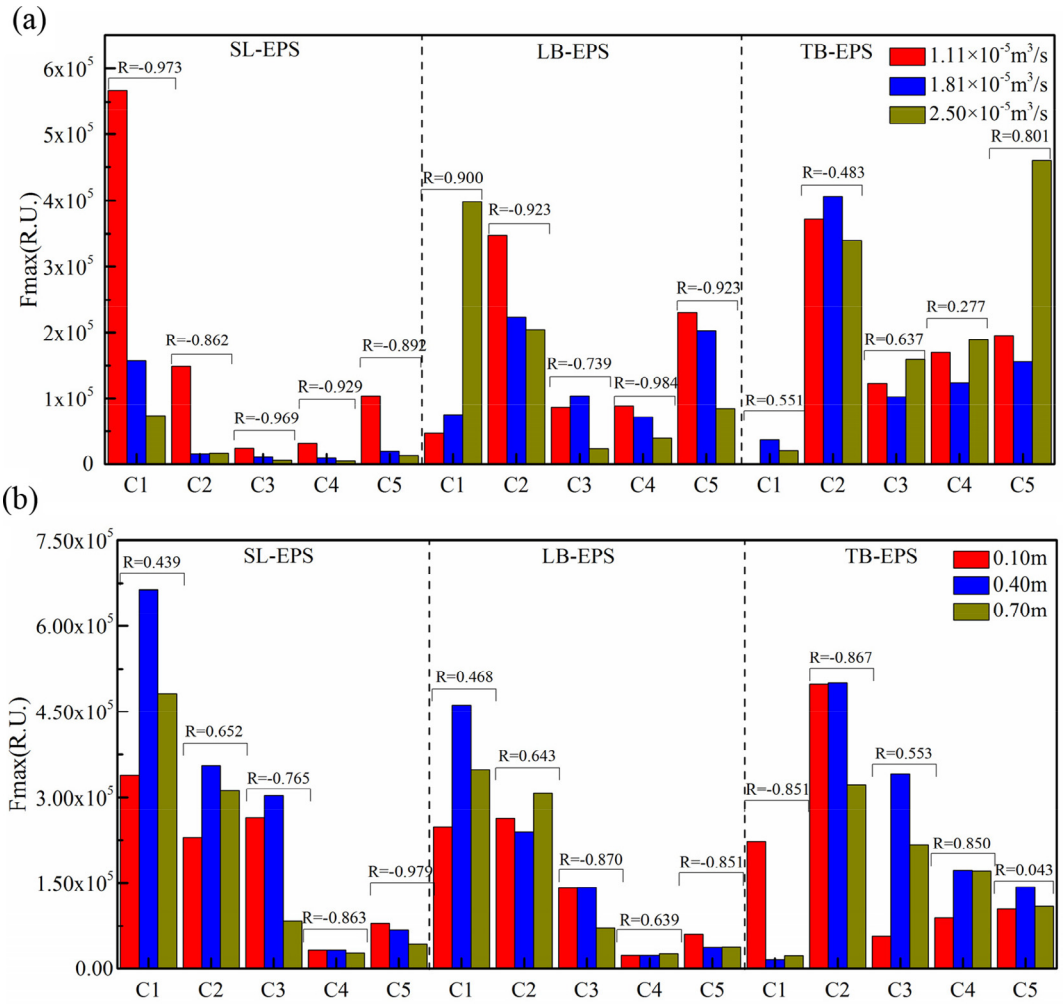

Fig. 4. Distribution of the maximum fluorescence intensity (Fmax) in the EPS matrix at different aeration rates and filter medium heights: (a) Aeration rates; (b) Filter medium heights.

according to previous studies (Cao et al., 2018; Ishii and Boyer, 2012; Qu et al., 2012; Wei et al., 2017).

3.4. PARAFAC analysis of EEM spectra

The maximum fluorescence intensities (Fmax) of the three EPS fractions obtained under different UBAF reactor conditions are shown in Fig. 4. The fluorescence intensity of the components of each EPS fraction was affected by the various aeration rates and filter medium heights. For the different aeration rates, the Fmax values of the protein-like substances (C1 and C2) in each EPS fraction were basically higher than those of the humic acid-like substance (Fig. 4(a)). The results were similar to those of Maqbool et al. (2016). The Fmax values of C2, C3, C4, and C5 in SL-EPS and LB-EPS had a significant negative correlation ($-0.984 \le R \le -0.739$, $1.512 \times 10^{-6} \le p \le 0.023$) with the aeration rates. A high aeration formed high turbulence, which could reduce the EPS contents. C1 in SL-EPS also showed a significant negative correlation ($R = -0.934$, $p = 2.224 \times 10^{-4}$) with the aeration rate, whereas C1 in LB-EPS showed the opposite trend ($R = 0.900$, $p = 9.432 \times 10^{-4}$). Abu Bakar et al. (2018) indicated that a high aeration rate impacted the production of EPS in biofilm. The high C1 content would help the biofilm to increase its detachment resistance in order to withstand the shearing force and to stabilize its structure. In addition, there was no significant correlation between the fluorescence intensity of the five components in TB-EPS and the aeration rates. The Fmax values of C2, C3, C4, and C5 in TB-EPS were significantly higher than those in SL-EPS and LB-EPS. The humic acid-like components (C3, C4, and C5) were higher at the aeration rate of 2.5×10^{-5} m^3/s than at 1.11×10^{-5} m^3/s and 1.81×10^{-5} m^3/s. The results showed that the high humic acid-like components of TB-EPS could be beneficial for stabilizing the biofilm structure under high aeration rates.

The Fmax distributions of each EPS fraction at different filter medium heights were similar to the distributions at various aeration rates (Fig. 4(b)). The contents of protein-like substances (C1 and C2) were significantly higher than those of humic-like substances (C3, C4, and C5) in SL-EPS and LB-EPS. Moreover, the Fmax of C2 in TB-EPS was higher than that of the other fluorescent substances. The results were consistent with the EPS fraction concentration. However, the Fmax of C1 in TB-EPS was significantly lower than that of the other substances. The difference in microbial metabolic activity might have affected the distributions of Fmax, as previously shown in another study (Miao et al., 2018). The filter medium heights showed a significant negative correlation ($-0.979 \le R \le -0.765$, $4.634 \times 10^{-6} \le p \le 0.016$) with the humic-like substances (C3, C4, and C5) of SL-EPS, the humic-like substances (C3 and C5) of LB-EPS, and the protein-like substances (C1 and C2) of TB-EPS, whereas they did not show a correlation with the other fluorescent substances. These results were related to the differences in the shearing force of the ceramsite surface and the metabolic activity of the microbial community.

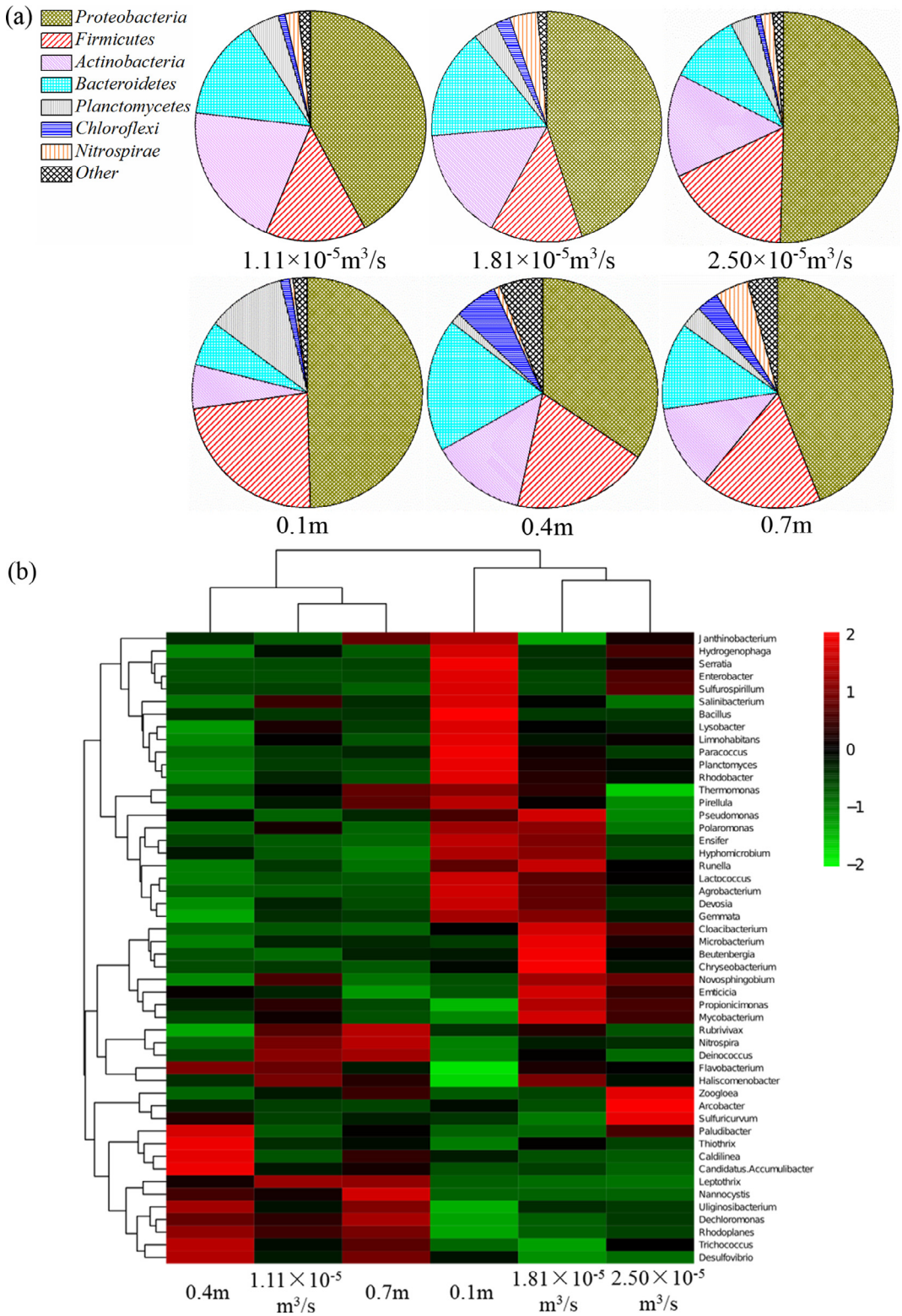

Fig. 5. Microbial community structures at different aeration rates and filter medium heights at the phylum and genus levels: (a) Relative abundance of the phyla at different conditions; (b) Heat-map distribution of the genus-level community composition combined with cluster analysis at different aeration rates and filter medium heights: Red represents a high relative abundance of the genus in the sample; green represents a lower abundance. (For interpretation of the references to colour in this figure legend, the reader is referred to the web version of this article.)

3.5. Microbial community composition

To explore the relationship between the EPS and the microbial community, the relative abundance of the microbes at the phylum and genus levels were determined (Fig. 5). At the phylum level (Fig. 5(a)), *Proteobacteria* (34.4%–50.4%) was the phylum with the highest abundance in all samples, followed by *Firmicutes* (12.7%–23.1%), *Actinobacteria* (6.2%–20.5%), *Bacteroidetes* (6.3%–18.7%), and *Planctomycetes*

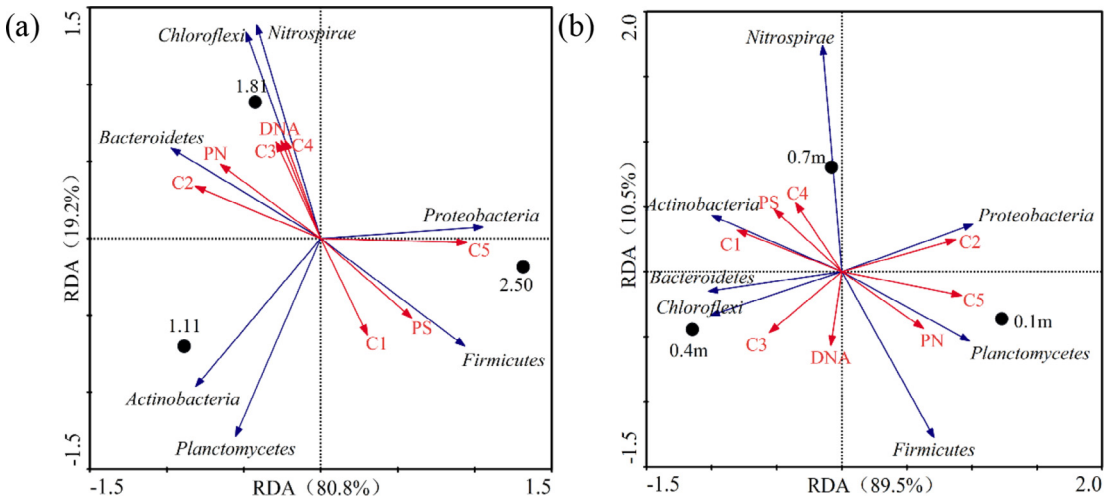

Fig. 6. Redundancy analysis between the EPS distribution and microbial community structure under different aeration rates and filter medium heights: (a) Aeration rates 1.11, 1.81, and 2.50 represent the aeration rates of $1.11 \times 10^{-5}\,m^3/s$, $1.81 \times 10^{-5}\,m^3/s$, and $2.50 \times 10^{-5}\,m^3/s$, respectively; (b) Filter medium heights.

(1.5%–11.0%). The results were generally consistent with those reported by Tao et al. (2016), with the exception that the relative abundance of *Proteobacteria* was lower in their study, likely because of differences in the reactor structure and microbial growth environment between the studies. The microbial community structure changed with the increase in aeration rates. The relative abundance of *Proteobacteria* had a significant positive correlation with the aeration rates, which was likely because the high aeration rate provided an adequate supply of dissolved oxygen for the activity and growth of the *Proteobacteria*. Previous studies have reported that the phylum *Proteobacteria* could convert nitrite to nitrate and remove phosphorus in the biological treatment of wastewater (Isanta et al., 2015). The relative abundance of *Planctomycetes* gradually decreased with the increase of the aeration rate from $1.11 \times 10^{-5}\,m^3/s$ to $2.50 \times 10^{-5}\,m^3/s$. Mulder et al. (1995) identified the *Planctomycetes* as being anaerobic ammonium-oxidizing bacteria, which could convert NH_4^+-N directly into N_2.

Compared with the structure under the different aeration rates, the microbial community structure showed a significant difference with the increase in filter medium heights (Fig. 5(a)). At the bottom of the filter medium layer, the relative abundance of *Proteobacteria*, *Firmicutes*, and *Planctomycetes* reached to 49.6%, 23.1%, and 11.0%, respectively, which was significantly higher than that at the other heights. These results were mainly related to the organic matter concentration and biofilm growth environment. Previous studies found that the dissolved oxygen concentration at the bottom of the filter medium layer was lower than that at other heights (Ren et al., 2018a). This condition would contribute to the growth of *Planctomycetes*. In addition, the high organic matter concentration at the filter medium height of 0.1 m could provide adequate nutrients for the growth of heterotrophic microorganisms (including *Proteobacteria*, *Firmicutes*, etc.). The metabolism of these bacteria was improved in this condition. At the top of the filter medium layer, the relative abundance of *Nitrospirae* (4.7%) was significantly higher than that at the other heights. As indicated by Pereira et al. (2014), the *Nitrospirae* belong to the nitrite-oxidizing bacteria, and a high dissolved oxygen concentration could increase the growth of these bacteria.

At the genus level (Fig. 5 (b)), the microbial community structure was significantly different at the various aeration rates and filter medium heights. Genera with a high abundance at $1.11 \times 10^{-5}\,m^3/s$ showed a significant change when the aeration rate was increased to $2.50 \times 10^{-5}\,m^3/s$ in Fig. 5(b). Under the aeration rate of $1.11 \times 10^{-5}\,m^3/s$, the highly abundant genera mainly appeared in the upper part of the figure. When the aeration rate was $1.81 \times 10^{-5}\,m^3/s$, the relative abundance of the genera was uniform and the microbial community structure was similar to that at the aeration rate of $2.50 \times 10^{-5}\,m^3/s$. The result was mainly related to the supply of dissolved oxygen and the aeration-causing shearing force. With the increase in the filter medium height, the microbial community structure changed significantly. The distribution of genera in high abundance at the filter medium height of 0.1 m was basically consistent with the distribution at the aeration rate of $1.11 \times 10^{-5}\,m^3/s$. Under the filter medium heights of 0.4 m and 0.7 m, the genera in high abundance were mainly concentrated in the lower part of the figure. This distribution was because the lower dissolved oxygen concentration and higher organic matter contents could affect the distribution of the microbial community structure. Furthermore, the different distributions of the microbial community structure could lead to changes in the EPS concentration, the relationship between these two parameters was further analyzed by RDA.

3.6. Relationship between microbial community and EPS distribution

In the RDA graph, the first axis explained 80.8% and 89.5% of the variance in the microbial community structure at the different aeration rates and filter medium heights, and the second axis explained the variance by 19.2% and 10.5%, respectively (Fig. 6). In Fig. 6, when the angle between two angles is < 90°, the smaller angle implies a stronger positive correlation. A greater angle (more than 90°) indicates a stronger negative correlation. Moreover, the arrow length represents the importance of the parameter (Zhang et al., 2018). The relative abundance of *Nitrospirae*, *Chloroflexi*, *Planctomycetes*, and *Actinobacteria* was of important for the variation in aeration rates. In addition, in the different filter medium heights, *Nitrospirae* and *Firmicutes* were important parameters. The results were consistent with the microbial community distributions under different reactor conditions. For the different aeration rates (Fig. 6(a)), the relative abundance of *Proteobacteria* had a significant positive relationship with the C5, C1, and PS contents, whereas it had a significant negative relationship with the C2, PN, C3, C4, and DNA contents. In contrast, *Nitrospirae*, *Chloroflexi*, and *Bacteroidetes* showed the opposite relationship compared with the *Proteobacteria*.

The relationship between the microbial community structure and the EPS compositions at different filter medium heights was significantly different compared with that at the different aeration rates (Fig. 6(b)). The relative abundance of *Proteobacteria* and *Planctomycetes* had significant positive correlation with the C2, C5, and PN contents, whereas they had significant negative correlation with the C1, PS, and C4 contents. In addition, *Nitrospirae* had significant positive correlation

with the C4 and PS contents. These results indicated that the difference in microbial community structure affected the concentration and compositional distributions of EPS at different environmental conditions. However, this study failed to systematically investigate the relationship between the EPS composition and the microbial community structure. Therefore, in order to reveal the details of this relationship, further work is needed to analyze the sources of EPS. In-depth research will help understanding the mechanism of pollutant removal and to conduct a better application of the UBAF reactor.

4. Conclusions

The relationships between the EPS and microbial community structures at different aeration rates and filter medium heights were explored. The results showed that the variation in aeration rates significantly ($R \leq -0.744$ & $R \geq 0.898$, $p \leq 0.022$) affected the EPS distribution. EEM-PARAFAC analysis indicated that the Fmax values of protein-like substances (C1 and C2) were consistently more dominant than those of humic-like components (C3, C4, and C5). Functional microorganisms (*Proteobacteria*, *Planctomycetes*, and *Nitrospirae*) were detected in all samples. The microorganisms showed a significant correlation with the contents of PN, PS, DNA, and fluorescent substances of EPS in the UBAF reactor.

Acknowledgements

This work was supported by the National Natural Science Foundation of China (NSFC) (No. 51679192).

Appendix A. Supplementary data

Supplementary data to this article can be found online at https://doi.org/10.1016/j.biortech.2019.121664.

References

Abu Bakar, S.N.H., Abu Hasan, H., Mohammad, A.W., Sheikh Abdullah, S.R., Haan, T.Y., Ngteni, R., Yusof, K.M.M., 2018. A review of moving-bed biofilm reactor technology for palm oil mill effluent treatment. J. Cleaner Prod. 171, 1532–1545. https://doi.org/10.1016/j.jclepro.2017.10.100.

Abu Hasan, H., Sheikh Abdullah, S.R., Kamarudin, S.K., Tan Kofli, N., Anuar, N., 2013. Simultaneous NH_4^+-N and Mn^{2+} removal from drinking water using a biological aerated filter system: effects of different aeration rates. Sep. Purif. Technol. 118, 547–556. https://doi.org/10.1016/j.seppur.2013.07.040.

Baghoth, S.A., Sharma, S.K., Amy, G.L., 2011. Tracking natural organic matter (NOM) in a drinking water treatment plant using fluorescence excitation-emission matrices and PARAFAC. Water Res. 45, 797–809. https://doi.org/10.1016/j.watres.2010.09.005.

Cao, B., Zhang, W., Du, Y., Wang, R., Usher, S.P., Scales, P.J., Wang, D., 2018. Compartmentalization of extracellular polymeric substances (EPS) solubilization and cake microstructure in relation to wastewater sludge dewatering behavior assisted by horizontal electric field: effect of operating conditions. Water Res. 130, 363–375. https://doi.org/10.1016/j.watres.2017.11.060.

Coble, P.G., 2007. Marine optical biogeochemistry: the chemistry of ocean color. Chem. Rev. 107, 402–418. https://doi.org/10.1021/cr050350+.

Flemming, H.-C., Wingender, J., Szewzyk, U., Steinberg, P., Rice, S.A., Kjelleberg, S., 2016. Biofilms: an emergent form of bacterial life. Nat. Rev. Microbiol. 14, 563–575. https://doi.org/10.1038/nrmicro.2016.94.

Flemming, H.-C., Wingender, J., 2010. The biofilm matrix. Nat. Rev. Microbiol. 8, 623–633. https://doi.org/10.1080/0892701031000072190.

He, Q., Gao, S., Zhang, S., Zhang, W., Wang, H., 2017. Chronic responses of aerobic granules to zinc oxide nanoparticles in a sequencing batch reactor performing simultaneous nitrification, denitrification and phosphorus removal. Bioresour. Technol. 238, 95–101. https://doi.org/10.1016/j.biortech.2017.04.010.

He, Q., Song, Q., Zhang, S., Zhang, W., Wang, H., 2018. Simultaneous nitrification, denitrification and phosphorus removal in an aerobic granular sequencing batch reactor with mixed carbon sources: reactor performance, extracellular polymeric substances and microbial successions. Chem. Eng. J. 331, 841–849. https://doi.org/10.1016/j.cej.2017.09.060.

Isanta, E., Bezerra, T., Fernández, I., Suárez-Ojeda, M.E., Pérez, J., Carrera, J., 2015. Microbial community shifts on an anammox reactor after a temperature shock using 454-pyrosequencing analysis. Bioresour. Technol. 181, 207–213. https://doi.org/10.1016/j.biortech.2015.01.064.

Ishii, S.K.L., Boyer, T.H., 2012. Behavior of reoccurring PARAFAC components in fluorescent dissolved organic matter in natural and engineered systems: a critical review. Environ. Sci. Technol. 46, 2006–2017. https://doi.org/10.1021/es2043504.

Keithley, S.E., Kirisits, M.J., 2018. An improved protocol for extracting extracellular polymeric substances from granular filter media. Water Res. 129, 419–427. https://doi.org/10.1016/j.watres.2017.11.020.

Liu, L., Huang, Q., Zhang, Y., Qin, B., Zhu, G., 2017. Excitation-emission matrix fluorescence and parallel factor analyses of the effects of N and P nutrients on the extracellular polymeric substances of Microcystis aeruginosa. Limnologica 63, 18–26. https://doi.org/10.1016/j.limno.2016.10.006.

Lu, F., Chang, C.H., Lee, D.J., He, P.J., Shao, L.M., Su, A., 2009. Dissolved organic matter with multi-peak fluorophores in landfill leachate. Chemosphere 74, 575–582. https://doi.org/10.1016/j.chemosphere.2008.09.060.

Maqbool, T., Quang, V.L., Cho, J., Hur, J., 2016. Characterizing fluorescent dissolved organic matter in a membrane bioreactor via excitation-emission matrix combined with parallel factor analysis. Bioresour. Technol. 209, 31–39. https://doi.org/10.1016/j.biortech.2016.02.089.

Miao, L., Zhang, Q., Wang, S., Li, B., Wang, Z., Zhang, S., Zhang, M., Peng, Y., 2018. Characterization of EPS compositions and microbial community in an Anammox SBBR system treating landfill leachate. Bioresour. Technol. 249, 108–116. https://doi.org/10.1016/j.biortech.2017.09.151.

Mulder, A., van de Graaf, A.A., Robertson, L.A., Kuenen, J.G., 1995. Anaerobic ammonium oxidation discovered in a denitrifying fluidized bed reactor. FEMS Microbiol. Ecol. 16, 177–183. https://doi.org/10.1016/0168-6496(94)00081-7.

Murphy, K.R., Hambly, A., Singh, S., Henderson, R.K., Baker, A., Stuetz, R., Khan, S.J., 2011. Organic matter fluorescence in municipal water recycling schemes: toward a unified PARAFAC model. Environ. Sci. Technol. 45, 2909–2916. https://doi.org/10.1021/es103015e.

Nagaraj, V., Skillman, L., Li, D., Ho, G., 2018. Review – Bacteria and their extracellular polymeric substances causing biofouling on seawater reverse osmosis desalination membranes. J. Environ. Manage. 223, 586–599. https://doi.org/10.1016/j.jenvman.2018.05.088.

Pereira, A.D., Leal, C.D., Dias, M.F., Etchebehere, C., Chernicharo, C.A.L., De Araújo, J.C., 2014. Effect of phenol on the nitrogen removal performance and microbial community structure and composition of an anammox reactor. Bioresour. Technol. 166, 103–111. https://doi.org/10.1016/j.biortech.2014.05.043.

Qu, F., Liang, H., He, J., Ma, J., Wang, Z., Yu, H., Li, G., 2012. Characterization of dissolved extracellular organic matter (dEOM) and bound extracellular organic matter (bEOM) of Microcystis aeruginosa and their impacts on UF membrane fouling. Water Res. 46, 2881–2890. https://doi.org/10.1016/j.watres.2012.02.045.

Ren, J., Cheng, W., Wan, T., Wang, M., Jiao, M., 2018a. Effect of aeration rates on hydraulic characteristics and pollutant removal in an up-flow biological aerated filter. Environ. Sci. Water Res. Technol. 4, 2041–2050. https://doi.org/10.1039/c8ew00231b.

Ren, J., Cheng, W., Wan, T., Wang, M., Zhang, C., 2018b. Effect of aeration rates and filter media heights on the performance of pollutant removal in an up-flow biological aerated filter. Water (Switzerland) 10, 8–10. https://doi.org/10.3390/w10091244.

Rezakazemi, M., Niazi, Z., Mirfendereski, M., Shirazian, S., Mohammadi, T., Pak, A., 2011. CFD simulation of natural gas sweetening in a gas-liquid hollow-fiber membrane contactor. Chem. Eng. J. 168, 1217–1226. https://doi.org/10.1016/j.cej.2011.02.019.

Seredyńska-Sobecka, B., Stedmon, C.A., Boe-Hansen, R., Waul, C.K., Arvin, E., 2011. Monitoring organic loading to swimming pools by fluorescence excitation-emission matrix with parallel factor analysis (PARAFAC). Water Res. 45, 2306–2314. https://doi.org/10.1016/j.watres.2011.01.010.

Shammi, M., Pan, X., Mostofa, K.M.G., Zhang, D., Liu, C.-Q., 2017. Seasonal variations and characteristics differences in the fluorescent components of extracellular polymeric substances from mixed biofilms in saline lake. Sci. Bull. 62, 764–766. https://doi.org/10.1016/j.scib.2017.04.016.

Shao, L., He, P., Yu, G., He, P., 2009. Effect of proteins, polysaccharides, and particle sizes on sludge dewaterability. J. Environ. Sci. 21, 83–88. https://doi.org/10.1016/S1001-0742(09)60015-2.

Sheng, G.P., Xu, J., Luo, H.W., Li, W.W., Li, W.H., Yu, H.Q., Xie, Z., Wei, S.Q., Hu, F.C., 2013. Thermodynamic analysis on the binding of heavy metals onto extracellular polymeric substances (EPS) of activated sludge. Water Res. 47, 607–614. https://doi.org/10.1016/j.watres.2012.10.037.

Sheng, G.P., Yu, H.Q., 2006. Characterization of extracellular polymeric substances of aerobic and anaerobic sludge using three-dimensional excitation and emission matrix fluorescence spectroscopy. Water Res. 40, 1233–1239. https://doi.org/10.1016/j.watres.2006.01.023.

Sheng, G.P., Yu, H.Q., Li, X.Y., 2010. Extracellular polymeric substances (EPS) of microbial aggregates in biological wastewater treatment systems: a review. Biotechnol. Adv. 28, 882–894. https://doi.org/10.1016/j.biotechadv.2010.08.001.

Shi, Y., Huang, J., Zeng, G., Gu, Y., Chen, Y., Hu, Y., Tang, B., Zhou, J., Yang, Y., Shi, L., 2017. Exploiting extracellular polymeric substances (EPS) controlling strategies for performance enhancement of biological wastewater treatments: an overview. Chemosphere 180, 396–411. https://doi.org/10.1016/j.chemosphere.2017.04.042.

Stedmon, C.A., Bro, R., 2008. Characterizing dissolved organic matter fluorescence with parallel factor analysis: a tutorial. Limnol. Oceanogr. Meth. 6, 572–579. https://doi.org/10.4319/lom.2008.6.572.

Stedmon, C.A., Seredyńska-Sobecka, B., Boe-Hansen, R., Le Tallec, N., Waul, C.K., Arvin, E., 2011. A potential approach for monitoring drinking water quality from groundwater systems using organic matter fluorescence as an early warning for contamination events. Water Res. 45, 6030–6038. https://doi.org/10.1016/j.watres.2011.08.066.

Tao, C., Peng, T., Feng, C., Chen, N., Hu, Q., Hao, C., 2016. The feasibility of an up-flow partially aerated biological filter (U-PABF) for nitrogen and COD removal from domestic wastewater. Bioresour. Technol. 218, 307–317. https://doi.org/10.1016/j.biortech.2016.06.098.

Wang, B.B., Liu, X.T., Chen, J.M., Peng, D.C., He, F., 2018. Composition and functional group characterization of extracellular polymeric substances (EPS) in activated sludge: the impacts of polymerization degree of proteinaceous substrates. Water Res. 129, 133–142. https://doi.org/10.1016/j.watres.2017.11.008.

Wei, L., An, X., Wang, S., Xue, C., Jiang, J., Zhao, Q., Kabutey, F.T., Wang, K., 2017. Effect of hydraulic retention time on deterioration/restarting of sludge anaerobic digestion: extracellular polymeric substances and microbial response. Bioresour. Technol. 244, 261–269. https://doi.org/10.1016/j.biortech.2017.07.110.

Xu, H., Cai, H., Yu, G., Jiang, H., 2013. Insights into extracellular polymeric substances of cyanobacterium Microcystis aeruginosa using fractionation procedure and parallel factor analysis. Water Res. 47, 2005–2014. https://doi.org/10.1016/j.watres.2013.01.019.

Yang, K., Yue, Q., Kong, J., Zhao, P., Gao, Y., Fu, K., Gao, B., 2016. Microbial diversity in combined UAF-UBAF system with novel sludge and coal cinder ceramic fillers for tetracycline wastewater treatment. Chem. Eng. J. 285, 319–330. https://doi.org/10.1016/j.cej.2015.10.019.

Yang, S., Li, X., 2009. Influences of extracellular polymeric substances (EPS) on the characteristics of activated sludge under non-steady-state conditions. Process Biochem. 44, 91–96. https://doi.org/10.1016/j.procbio.2008.09.010.

Yu, G.H., He, P.J., Shao, L.M., 2009. Characteristics of extracellular polymeric substances (EPS) fractions from excess sludges and their effects on bioflocculability. Bioresour. Technol. 100, 3193–3198. https://doi.org/10.1016/j.biortech.2009.02.009.

Yu, H., Qu, F., Sun, L., Liang, H., Han, Z., Chang, H., Shao, S., Li, G., 2015. Relationship between soluble microbial products (SMP) and effluent organic matter (EfOM): characterized by fluorescence excitation emission matrix coupled with parallel factor analysis. Chemosphere 121, 101–109. https://doi.org/10.1016/j.chemosphere.2014.11.037.

Zhang, L., Zhang, J., Zeng, G., Dong, H., Chen, Y., Huang, C., Zhu, Y., Xu, R., Cheng, Y., Hou, K., Cao, W., Fang, W., 2018. Multivariate relationships between microbial communities and environmental variables during co-composting of sewage sludge and agricultural waste in the presence of PVP-AgNPs. Bioresour. Technol. 261, 10–18. https://doi.org/10.1016/j.biortech.2018.03.089.

Zhang, W., Yang, P., Xiao, P., Xu, S., Liu, Y., Liu, F., Wang, D., 2015. Dynamic variation in physicochemical properties of activated sludge floc from different WWTPs and its influence on sludge dewaterability and settleability. Colloids Surf., A 467, 124–134. https://doi.org/10.1016/j.colsurfa.2014.11.027.

Zhu, L., Yu, Y., Dai, X., Xu, X., Qi, H., 2013. Optimization of selective sludge discharge mode for enhancing the stability of aerobic granular sludge process. Chem. Eng. J. 217, 442–446. https://doi.org/10.1016/j.cej.2012.11.132.